Mon. Not. R. Astron. Soc. **372,** 551–564 (2006) doi:10.1111/j.1365-2966.2006.10855.x

Magnetic field inclination and atmospheric oscillations above solar active regions

H. Schunker★ and P. S. Cally★

Centre for Stellar and Planetary Astrophysics, School of Mathematical Sciences, Monash University, Victoria 3800, Australia

Accepted 2006 July 24. Received 2006 July 21; in original form 2006 May 25

ABSTRACT

Recent observational evidence for magnetic field direction effects on helioseismic signals in sunspot penumbrae is suggestive of magnetohydrodynamic (MHD) mode conversion occurring at lower levels. This possibility is explored using wave mechanical and ray theory in a model of the Sun's surface layers permeated by uniform inclined magnetic field. It is found that fast-to-slow conversion near the equipartition depth at which the sound and Alfvén speeds coincide can indeed greatly enhance the atmospheric acoustic signal at heights observed by Solar and Heliospheric Observatory/Michelson Doppler Imager and other helioseismic instruments, but that this effect depends crucially on the wave *attack angle*, i.e. the angle between the wavevector and the magnetic field at the conversion/transmission depth. A major consequence of this insight is that the magnetic field acts as a filter, preferentially allowing through acoustic signal from a narrow range of incident directions. This is potentially testable by observation.

Key words: MHD – Sun: helioseismology – Sun: magnetic fields – sunspots.

1 INTRODUCTION

The solar interior is awash with acoustic waves, propagating through every region, both deep and shallow. Refraction due to the increasing sound speed with depth inevitably sees them emerge at the surface, where they may be observed and interrogated by helioseismologists. Global helioseismology, where spherical or at least axial symmetry is normally assumed, is traditionally carried out in the context of a spherical harmonic modal expansion, with the fundamental constituents of the wave field taken to be the f and p modes familiar from a normal mode analysis of the linearized stellar pulsation equations (Unno et al. 1989), and consistently observed on the Sun for several decades now.

Not content with probing the Sun's global structure, helioseismologists in more recent times have focused attention on local features, most prominently active regions, including sunspots. Some of the first such studies (e.g. Braun et al. 1987; Bogdan et al 1993; Braun 1995) retained the modal perspective, and decomposed the observed surface oscillations in annuli around sunspots into incoming and outgoing f and p modes (the Hankel analysis), to reveal that the spots partially absorb wave energy and shift their phase. Developing an original idea of Spruit (1991), that near-surface conversion to slow magnetoacoustic waves is responsible for the absorption, a long line of theoretical development (Spruit & Bogdan 1992; Cally & Bogdan 1993; Cally, Bogdan & Zweibel 1994; Bogdan & Cally 1997; Rosenthal & Julian 2000; Crouch 2003; Crouch & Cally 2003, 2005; etc.), culminating in some impressive comparisons with the observational absorption and phase shift data (Cally, Crouch & Braun 2003; Crouch et al. 2005), has demonstrated the feasibility of the mechanism. Most significantly, for our purposes here, we conclude that, in the near-surface layers where the Alfvén speed can become comparable to or exceed the sound speed, active region magnetic field substantially alters the behaviour of helioseismic signals emerging from below.

However, more modern local helioseismic techniques, such as time–distance analysis (D'Silva 1996; Kosovichev, Duvall & Scherrer 2000) and acoustic holography (Braun & Lindsey 2000), eschew normal mode decomposition in favour of ray or local wave field descriptions. To understand how Spruit's mechanism operates in this context, Cally (2005) used a perturbation approach to examine mode coupling and conversion of a simple acoustic (fast) wave approaching a 'sunspot' from below in an idealized vertical field polytropic model. The perturbation variable was effectively the angle of propagation of the wave away from vertical. It was found that fast and slow magnetoacoustic waves couple to greater or lesser extent in the neighbourhood of the equipartition level $z_{\rm eq}$ where the sound and Alfvén speeds coincide, $c = a$, and that the fast-to-slow transmission coefficient T depends sensitively on this approach angle, with greater transmission when it is fine.

Subsequently, Cally (2006) greatly extended the applicability of such analyses by adopting a generalized ray theoretic description in place of the perturbation method, utilizing the mathematical mode conversion formalism of Tracy, Kaufman & Brizard (2003).[1] In

★E-mail: hannah.schunker@sci.monash.edu.au (HS); paul.cally@sci.monash.edu.au (PSC)

[1] There is a very extensive literature on mode conversion in the plasma physics literature; see e.g. the monograph by Swanson (1998) and the series

the restricted case of the vertical field polytrope, the two methods agree. However, arbitrary thermal and magnetic models become tractable with the new method. One purpose of this paper is to further develop the coupled ray approach and apply it to more realistic models to fully explore the conditions under which mode conversion will occur in the real Sun and predict how this will manifest itself at observational heights. The other is to begin an interpretation of recent observational evidence for near-surface influence of sunspot magnetic field *direction* on helioseismic signals (Schunker et al. 2005).

Hankel and some other local helioseismic probings of sunspots utilize only data taken from regions *surrounding* the spot, and not from within it. This is to be recommended to some extent, as it avoids several observational difficulties and theoretical uncertainties. Nevertheless, eventually one must try to compare expectations with what is actually observed *within* sunspots. At this stage, such studies have mainly been restricted to penumbrae because of signal-to-noise ratio issues in umbrae, but it is to be hoped that these can be overcome shortly.

Using up to 10 consecutive days' line-of-sight Doppler velocity data from the Michelson Doppler Imager (MDI) aboard the Solar and Heliospheric Observatory (SOHO) spacecraft, and vector magnetograms from the Imaging Vector Magnetograph (IVM; Mickey et al. 1996), Schunker et al. (2005, 2006) were able to analyse the significance of magnetic field direction in sunspot penumbrae to helioseismic signals by utilizing the passage of the spots across the solar disc to effectively achieve a multitude of viewing angles. Their prime tool was the local control correlation of the acoustic ingression H_- and the observed line-of-sight Doppler velocity ψ,

$$C(\nu) = \langle \hat{H}_-(\boldsymbol{r}, \nu)\hat{\psi}^*(\boldsymbol{r}, \nu)\rangle_{\Delta\nu}, \quad (1)$$

where $\boldsymbol{r}$ is the position, ν is the frequency, the asterisk denotes complex conjugation and the average is over a frequency range $\Delta\nu$ (typically 1 mHz centred at either 3, 4 or 5 mHz). The hats indicate temporal Fourier transforms. Broadly, the idea is that surface oscillations are primarily due to driving by incoming acoustic waves which can be seen in an annular pupil about the point of interest at an earlier time, and that the acoustic ingression represents this driving term. With this assumed, C should be closer to unity in the quiet Sun than in active regions, though the intrinsic limitations of holography leave a significant residual $1 - C$ even in the most ideal quiet regions. Magnetic effects on helioseismic signals are therefore quantified by the increasing departure of C from 1 as magnetic field strength increases, and with variation of magnetic field inclination. Both $|C|$ and $\delta\phi = \arg C$ yield useful insights, with the latter in particular being sensitive to traveltime variations.

In viewing the penumbra from various angles, binned according to field inclination to the vertical (which is anticorrelated with field strength), it is found that there is a substantial average (negative) $\delta\phi$. As expected, $|\delta\phi|$ decreases with increasing field inclination (decreasing field strength). In part, this could reflect the decreasing thermal effect of the spot, or the decreasing depth of the Wilson depression, which affect sound speed and path length,[2] respectively. However, there is also a statistically significant dependence on the projected line-of-sight angle θ_p (the inclination of the line-of-sight projected on to the vertical plane containing the magnetic field), which argues for a description beyond the purely acoustic. Conversion is extremely sensitive to the magnetic field direction at the z_{eq} layer. Slow wave propagation relies heavily on guidance by the magnetic field, and the results of Schunker et al. (2005) lead us to conclude that this is implicated in observed penumbral oscillations.

Unravelling the mysteries of near-surface magnetic influence on helioseismic waves involves first and foremost determining the relativities of several heights: the equipartition level z_{eq} where $a = c$ and near where mode conversion typically occurs; the height of formation $z_{676.8}$ of the 676.8-nm Ni I spectral line used by MDI and also by GONG (Global Oscillations Network Group); and the cut-off level $z_c(\nu)$ at which an upcoming acoustic wave of frequency ν reflects back downward (if at all) off the increasing acoustic cut-off frequency. We hold as self-evident that white light penumbrae are magnetically dominated, else they would not exhibit such pronounced fibril structure. Since $z_{676.8}$ is about 200 km above optical depth unity ($\tau_{0.5} = 1$), we will assume that this region therefore also has $a > c$. Furthermore, the inversions of Mathew et al. (2004) based on two infrared Fe I lines formed 20–30 km deeper than $\tau_{0.5} = 1$ find that even there, most of the penumbra has a plasma beta [$\beta = p_{gas}/p_{mag} = (2/\gamma)\, c^2/a^2$] less than 1, and parts of the outer regions only reaching about 1.5–1.8 (see their fig. 8d). Taking all these pieces of evidence into account, we may safely assume that $z_{eq} < z_{676.8}$ in sunspots.

However, what of z_c? If $z_c < z_{eq}$ the upcoming fast (acoustic) wave would reflect before undergoing any mode conversion, or taking on any substantial magnetic characteristics. However, the success of mode conversion theory in modelling the Hankel absorption and phase shift data in inclined magnetic field (Cally et al. 2003; Crouch et al. 2005) suggests that at least in some substantial portion of a sunspot, containing significantly inclined field ($\theta \gtrsim 20^\circ$), the waves must be reaching the conversion (equipartition) depth. The additional fact that magnetic directional influences are apparent in the observed correlation phase (Schunker et al. 2005) further suggests that $a \gtrsim c$ at the height of formation of the MDI 676.8-nm Ni I line, and that the wave has not reflected off the acoustic cut-off before reaching z_{eq}, at least at 3 mHz and above. Further evidence for mode conversion is found in coronal loops, where 6-mHz slow magnetoacoustic waves originating from below have been identified (Brynildsen et al. 2002; De Moortel, Ireland & Walsh 2002).

The structure of this paper is as follows. Section 2 introduces the model atmosphere we will use throughout, and discusses a subtle but important point regarding the acoustic cut-off frequency. Section 3 presents a simple numerical experiment which clearly shows the importance of magnetic field inclination in determining the helioseismic signal penetrating to the overlying atmosphere of a sunspot. A magnetic modification of the well-known GONG Model S of Christensen-Dalsgaard et al. (1996) is used throughout to represent the surface layers of the Sun. Section 4 sets up a new implementation of magnetohydrodynamic (MHD) ray coupling theory based on the variational formulation of linear MHD wave theory. Section 5 applies ray coupling theory to explain and illuminate the numerical wave mechanical results of Section 3. Section 6 presents our final conclusions.

2 ATMOSPHERE AND CONVENTIONAL WAVE EQUATION

A commonly used representation of the wave equations in a *non*-magnetic plane-stratified atmosphere (Deubner & Gough 1984;

of papers by Cairns & Lashmore-Davies (1983, 1986) and Cairns & Fuchs (1989). The various mathematical approaches found therein are all of course related. However, for our purposes, the formalism of Tracy et al. (2003) is most convenient because of its generality and elegant structure.

[2] Though see the model of Appendix A where the Wilson depression does not alter the depth of acoustic reflection produced by the acoustic cut-off frequency.

Balmforth & Gough 1990) is

$$\frac{\mathrm{d}^2\Psi}{\mathrm{d}z^2} + \left(\frac{\omega^2 - \omega_\mathrm{c}^2}{c^2} + \frac{N^2}{\omega^2}k_x^2 - k_x^2\right)\Psi = 0, \tag{2}$$

where $\Psi = \rho^{1/2}\, c^2\, \nabla \cdot \boldsymbol{\xi}$ represents the acoustic field, $\boldsymbol{\xi} = (\xi, 0, \zeta)$ is the displacement vector, ω is the wave frequency, k_x is the horizontal wavenumber and ω_c and N are the acoustic cut-off and Brunt–Väisälä frequencies, respectively, defined by

$$\omega_\mathrm{c}^2 = \frac{c^2}{4H^2}\left(1 - 2H'\right) \tag{3}$$

and

$$N^2 = \frac{g}{H} - \frac{g^2}{c^2}. \tag{4}$$

Here, $H(z) = -\rho(z)/\rho'(z)$ is the density scaleheight. Equation (2) is formally in very convenient form for deciding where the solution is oscillatory, and for application of the standard Wentzel–Kramers–Brillouin (WKB) theory (Bender & Orszag 1978).

A convenient and widely utilized model of the solar interior is Model S of Christensen-Dalsgaard et al. (1996). This is modified as described in Appendix A to account for an imposed magnetic field. We term this the magnetically modified Model S (MMMS). The acoustic cut-off and Brunt–Väisälä frequencies are graphed as functions of height z in Fig. 1 for the non-magnetic case. They differ only slightly in the MMMS models. Schmitz & Fleck (1998, 2003) point out that the wave equation (2) is problematic for practical applications involving empirical atmospheric models, because of the sharp variation in ω_c near the surface. In particular, the WKB theory, where the coefficients are assumed to vary slowly compared with the dependent variable Ψ, is clearly inappropriate. Naive application of ray theory for example, which is based on a low-order (geometrical optics) application of the WKB theory, would predict that a 6-mHz ray (say) incident on the spike should totally reflect. However, simple wave mechanical modelling shows that the acoustic cut-off spike actually has a very minor effect on wave solutions at 6 mHz (Fig. 2), as they easily tunnel through it. There is certainly very little reflection from it.

Cally (2006) generalized equation (2) to include uniform inclined magnetic field, and developed a ray theoretic description of mode conversion based on it. This was appropriate for the simple polytropic atmospheres he treated, but clearly is not appropriate for realistic atmospheres such as Model S which exhibit the acoustic cut-off

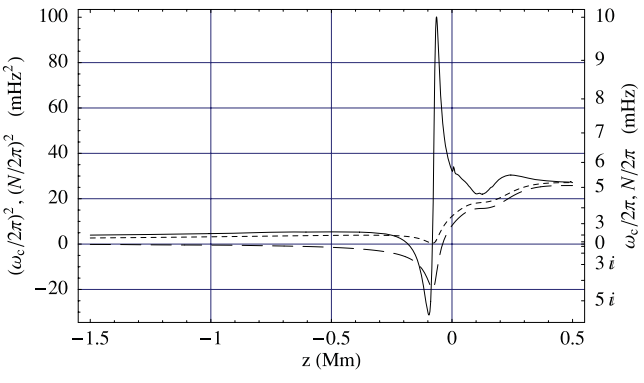

Figure 1. The acoustic cut-off (full curve) and Brunt–Väisälä (long dashed) frequencies (mHz) from the Model S of Christensen-Dalsgaard et al. (1996). Note that both ω_c^2 and N^2 are negative at some depths, and so ω_c and N are imaginary there, as indicated in the labelling of the right-hand axis. The dotted curve represents the 'isothermal' acoustic cut-off $\omega_\mathrm{ci} = c/2H$, which is used extensively in Sections 4 and 5.

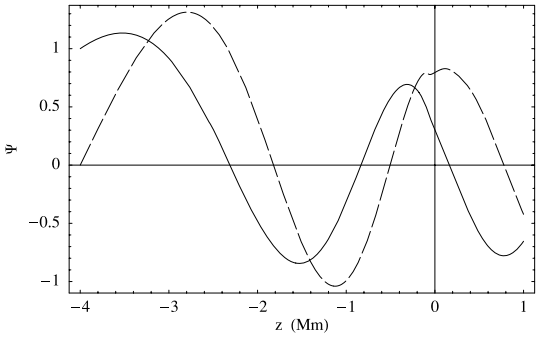

Figure 2. Numerical solution of equation (2) for a 6-mHz wave driven at $z = -4$ Mm in Model S, and with a radiation boundary condition at the top (real and imaginary parts as full and dashed curves, respectively). k_x is chosen so that the natural depth of the acoustic cavity for this mode is 5 Mm (i.e. the driver is inside the cavity). The effect of the acoustic cut-off spike at about −100 km is barely evident.

spike. Although Cally's equations may still be used (with care) for wave mechanical calculations, they are not advised for use with a ray description. As we present both wave mechanical and ray theoretic calculations here, we therefore choose *not* to use wave equations based on Ψ.

3 WAVE MECHANICAL EXPERIMENT

The question addressed here concerns the effect of magnetic field inclination on the two-dimensional propagation of waves in a plane-stratified (one-dimensional) atmosphere. In sunspots with diameters of several tens of megametres, but magnetic 'depths' of only a few hundred kilometres (depths over which the magnetic field is dynamically significant), magnetic field gradients may be expected to be of secondary importance (though see Khomenko & Collados 2006, for modelling of waves in a small sunspot where radial Alfvén speed gradients can produce significant refraction of the fast wave in the atmosphere). We therefore assume that the fields are (locally) uniform but inclined to the vertical. Typically, the inclination angle will be small in umbrae and large in penumbrae.

We examine the two-dimensional (x–z plane) propagation of magnetoacoustic waves in MMMS models with uniform inclined magnetic field. The governing linearized wave equations may be written in terms of the x and z displacements ξ and ζ:

$$a^2\cos^2\theta\left(\frac{\mathrm{d}^2}{\mathrm{d}z^2} - k_x^2\right)\xi + \left(\omega^2 - c^2k_x^2\right)\xi = a^2\cos\theta\sin\theta\left(\frac{\mathrm{d}^2}{\mathrm{d}z^2} - k_x^2\right)\zeta - \mathrm{i}k_x\left(c^2\frac{\mathrm{d}}{\mathrm{d}z} - g\right)\zeta \tag{5}$$

and

$$a^2\cos\theta\sin\theta\left(\frac{\mathrm{d}^2}{\mathrm{d}z^2} - k_x^2\right)\xi - \mathrm{i}k_x\left(c^2\frac{\mathrm{d}}{\mathrm{d}z} + \frac{\mathrm{d}c^2}{\mathrm{d}z} - \frac{c^2}{H} + g\right)\xi = \left[c^2\frac{\mathrm{d}^2}{\mathrm{d}z^2} + \left(\frac{\mathrm{d}c^2}{\mathrm{d}z} - \frac{c^2}{H}\right)\frac{\mathrm{d}}{\mathrm{d}z} + \omega^2\right]\zeta + a^2\sin^2\theta\left(\frac{\mathrm{d}^2}{\mathrm{d}z^2} - k_x^2\right)\zeta. \tag{6}$$

Here, a is the Alfvén speed.

These wave equations are solved numerically in $z_\mathrm{b} \leqslant z \leqslant z_\mathrm{t}$ subject to two boundary conditions at each endpoint. The base z_b is chosen to be quite deep, but still within the acoustic cavity (i.e. the term in bracket on the left-hand side of equation 2 is positive). At the

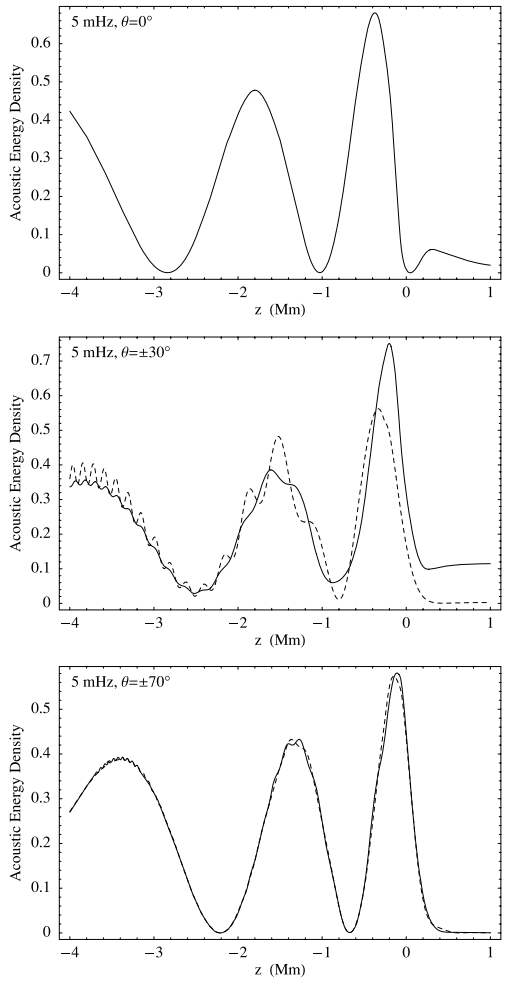

Figure 3. Acoustic energy density $|p_1|^2/2\rho c^2$ for 2-kG magnetic field inclined at 0° (top panel), ±30° and ±70° (bottom panel). In each case, the full curve corresponds to positive inclination θ, and the dotted curve to negative tilt. For all panels, the driving frequency is 5 mHz, the base of the acoustic cavity is at $z_1 = -5$ Mm, and the driver is at $z_b = -4$ Mm. The top is at $z_t = 1$ Mm.

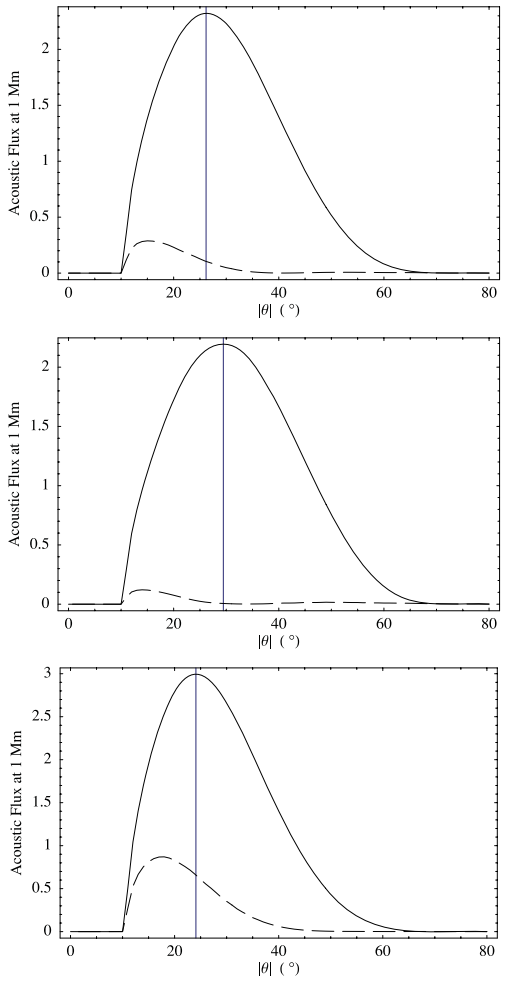

Figure 4. Top panel: acoustic wave energy vertical flux $F_{ac} = p_1\, w$ at $z = 1$ Mm as a function of magnetic field inclination θ for the case of Fig. 3. Middle panel: same, but for a shallower driver at $z = -2.5$ Mm in an acoustic cavity with base at $z_1 = -3$ Mm. Bottom panel: same, but for a driver at $z = -4$ Mm in an acoustic cavity with base at $z_1 = -10$ Mm. To emphasize the asymmetry between $\theta < 0$ and $\theta > 0$, the figures have been 'folded over' by plotting F_{ac} against $|\theta|$, with the full curve corresponding to positive θ and the dashed curve to negative θ. The vertical line indicates the angle at which the maximum flux occurs.

top, radiation or exponential decay (as appropriate) conditions are applied by matching on to exact solutions in the overlying isothermal atmosphere.[3] Finally, a slow wave radiation condition and a simple acoustic driver are applied at z_b. The solutions are normalized to have unit acoustic energy in $z_b < z < 0$. It is desired to determine the degree to which the acoustic field penetrates the 'photosphere'.

Fig. 3 depicts the acoustic energy density $E_{ac} = |p_1|^2/2\rho_0 c^2$, where p_1 is the Eulerian pressure perturbation, throughout the computational domain for 5-mHz oscillations in a model with 2-kG magnetic field inclined at angles $\theta = 0°$, ±30° and ±70° to the vertical. In the vertical field case, the energy in the overlying atmosphere $z > 0$ drops off exponentially with height, due to acoustic cut-off frequency in the atmosphere (5.2 mHz) exceeding the wave frequency. In inclined field though, the ramp effect (see Section 4) reduces the effective cut-off frequency by a factor $\cos\theta$ and the waves may propagate upward throughout, resulting in an asymptotically uniform acoustic energy density. A very great discrepancy is apparent though between the $\theta = 30°$ and $-30°$ cases, with the former exhibiting far greater power than the latter in $z > 0$. In each of the cases $\theta = \pm 30°$ and ±70°, the subsurface solution is little altered by a change of sign in field inclination, demonstrating that the large difference in the overlying atmosphere is a local effect. However, one clear distinction is the much greater amplitude in the small-scale (slow mode) oscillations in the $\theta = -30°$ case at $z \lesssim -3$ Mm compared to either $\theta = 30°$ or ±70°. This is due to greatly enhanced mode conversion to *downgoing* slow modes near the surface (see Figs 12 and 13, below).

Fig. 4 plots the acoustic wave energy flux $F_{ac} = p_1 w$, where $w = \partial\zeta/\partial t$ is the vertical component of velocity, reaching the top of the computational domain at $z = 1$ Mm. This is effectively asymptotic if the frequency exceeds the ramp acoustic cut-off frequency, and almost zero otherwise. The figure clearly illustrates this, displaying

[3] Exact solutions of the wave equations in terms of Meijer G-functions were derived by Zhugzhda & Dzhalilov (1982) for vertical field and Zhugzhda & Dzhalilov (1984) for inclined field. Simpler solutions in terms of ${}_2F_3$ hypergeometric functions were subsequently found by Cally (2001) and Crouch (private communication), respectively.

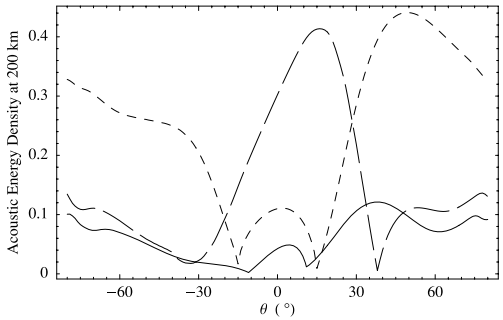

Figure 5. Acoustic energy density at $z = 200$ km for various angles of magnetic field inclination θ for three models. Full curve: 5-mHz oscillations in 2-kG magnetic field (the case of Figs 3 and 6); long dashed curve: 4 mHz and 2 kG; short dashed curve: 5 mHz and 1-kG field. In each case, all other parameters are as for Fig. 3.

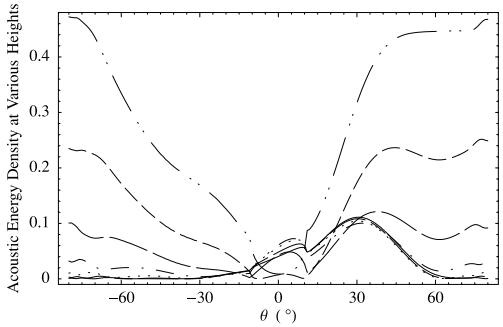

Figure 6. Acoustic energy density at $z = 0$, 100, 200, ... , 600 km (top to bottom) for various angles of magnetic field inclination θ for the case of 5-mHz oscillations in 2-kG magnetic field (cf. Fig. 3).

a rapid rise in flux beyond $\theta \approx 10^\circ$, as the acoustic waves undergo transition from evanescent to travelling. In the top panel (acoustic cavity depth of 5 Mm), a maximum flux is reached at around 26°, beyond which it declines, partly for geometrical reasons, but mostly because of diminishing fast-to-slow transmission near the $a = c$ equipartition point, as will become clear in Sections 4 and 5. A shallower acoustic cavity (middle panel) yields a slightly higher angle at which $F_{\rm ac}$ peaks ($\approx 29.5^\circ$), whilst a deeper cavity (bottom panel) produces a slightly lower angle at the peak. This will also be explained later using insights from the ray theory.

Fig. 5 plots the acoustic wave energy density at $z = 200$ km, corresponding roughly to the height observed by SOHO/MDI, as a function of θ for this and two other models. The central 'bulge' at small $|\theta|$ in each panel represents the regime where the acoustic waves in $z > 0$ are evanescent. This is naturally wider at lower frequency, as greater inclination is needed for the ramp effect to overcome the acoustic cut-off. Once the ramp effect kicks in, we again see that positive θ is favoured. At large inclinations, the enhancement effect is lost.

Fig. 6 plots the acoustic wave energy density against magnetic field inclination θ at various heights for the case of Fig. 3. We see that this falls with height for $|\theta| > \arccos(\omega/\omega_{\rm ci}) \approx 10.7^\circ$, but especially for positive θ, approaches an asymptotic state corresponding to unhindered slow mode propagation up the field lines.

In seeking to interpret observed oscillations at or near the solar surface, particularly in magnetic regions, polarization of the plasma motions is an important discriminant of wave type. For example, the basic magnetoacoustic wave theory indicates that the slow wave polarization is strongly field aligned when $a \gg c$, whereas the fast

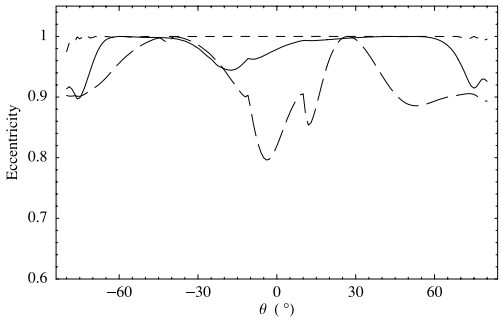

Figure 7. Velocity ellipse eccentricity at three heights for the model of Fig. 3 and various field inclinations θ. Full curve: $z = 200$ km; long dash: $z = 0$; short dash: $z = 1$ Mm.

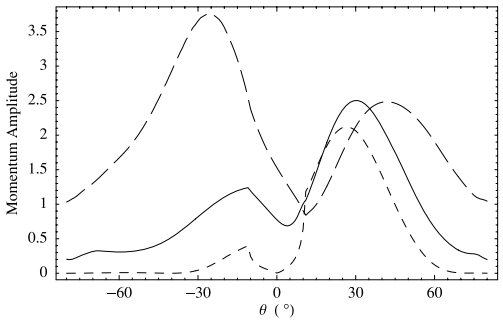

Figure 8. Semimajor axis length for momentum ellipses (i.e. velocity ellipses scaled by density) at three heights for the model of Fig. 3 and various field inclinations θ. Full curve: $z = 200$ km; long dash: $z = 0$; short dash: $z = 1$ Mm.

wave is not. However, velocity is not generally linearly polarized. In fact, at any particular height, an element of plasma undergoes elliptical motion about its equilibrium position, with the eccentricity and inclination of the ellipse dependent on the complex ratio $b = \zeta/\xi$. If ψ is the inclination of a principal axis of this ellipse, it is a simple matter to show that $\tan 2\psi = 2\,{\rm Re}\{b\}/(1 - |b|^2)$. The semimajor and semiminor axes, and hence the eccentricity, are also easily calculated. For comparison with observations, most notably Schunker et al. (2005, 2006), it is of interest to examine these quantities here for the models discussed above.

Figs 7–9 summarize the results for the model of Fig. 3. First, at the SOHO/MDI height of 200 km, the eccentricity (Fig. 7) is close to unity for all magnetic field inclinations, indicating almost rectilinear motion. As we might expect from the earlier results on acoustic energy density, it is apparent from Fig. 8 that $\theta > 0$ is favoured as regards velocity (or displacement or momentum) amplitude. Neither of these results applies at $z = 0$. The angle δ between the semimajor axis of the velocity ellipse and the magnetic field is effectively zero high enough in the atmosphere (Fig. 9), where only the (acoustic) slow wave remains, and is rigidly channelled by the magnetic field. However, it is found that δ deviates considerably from zero at the nominal SOHO/MDI observation height of around 200 km, suggesting a combination of loose acoustic channelling and remnant fast wave contribution. This result is expected to be extremely sensitive to the ratio of the Alfvén and sound speeds at each height (Fig. 10),[4]

[4] This fast growth of a^2/c^2 with height is predominantly due to the rapidly decreasing density, but is also partially a result of the incorrect assumption in the model that magnetic field strength is constant.

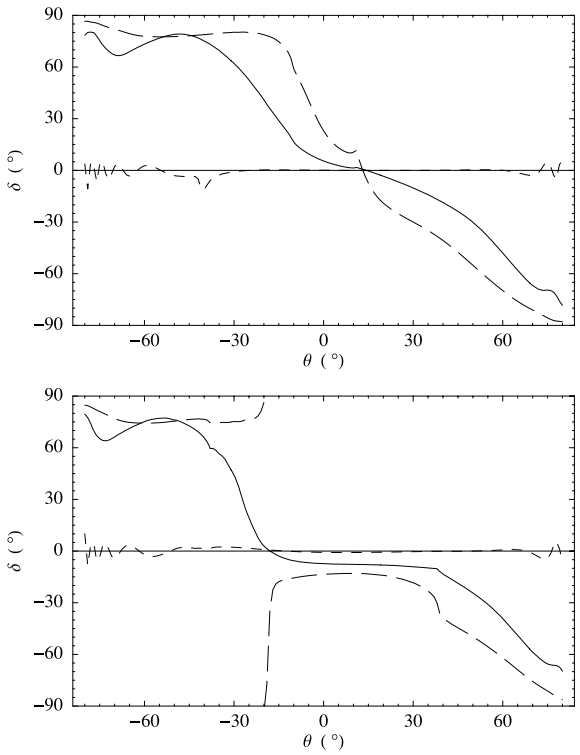

Figure 9. Top panel: the angle δ that the semimajor axis makes to the magnetic field at $z = 200$ km (full curve), $z = 0$ (long dashed curve), and $z = 1$ Mm (short dashed curve) for the model of Figs 3 and 8. Bottom panel: same, but for 4 rather than 5 mHz.

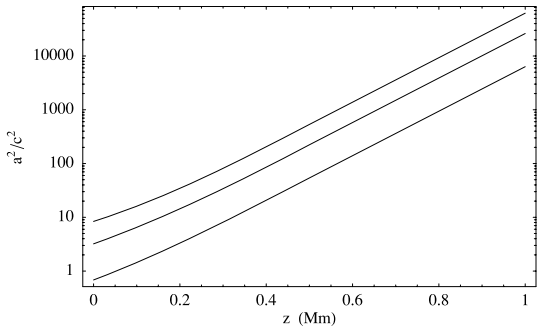

Figure 10. The ratio a^2/c^2 in the MMMS models with field strength 1 kG (bottom curve), 2 kG (middle) and 3 kG (top).

with more field alignment as the ratio increases. At $z = 200$ km in the 2-kG model, we have $a^2/c^2 = 14.2$ only, and so might not expect very strong channelling. By $z = 1$ Mm, it is 2.6×10^4, which clearly enforces very rigid acoustic channelling. Despite the moderate values of a^2/c^2 at 200 km and below, evanescent oscillations are found to be quite closely field aligned there (Fig. 9, lower panel; $-20^\circ \lesssim \theta \lesssim 35^\circ$).

In summary, Figs 7–9 emphasize that the fast mode diminishes in relative importance with height in the atmosphere, leaving the slow mode to dominate the oscillations, and to become progressively more tightly aligned with the magnetic field as a/c increases. However, this process is not complete at heights typically sampled by helioseismic instruments, leaving a fairly complex velocity polarization structure which may, on further study, provide useful insights when comparing theory with observation.[5]

The most significant result, though, is that somehow, magnetic field inclination *of a certain sense* opens a window into the overlying atmosphere for acoustic oscillations. This is potentially important for understanding the helioseismology of sunspots since observations (e.g. by MDI) are made in precisely these regions. To understand the cause of this effect, we turn to ray theory.

4 RAY CONVERSION THEORY

Although fully wave mechanical numerical solutions, such as those of the previous section, are easy to calculate, understanding of physics involved is advanced using a ray theoretic description. This is particularly true of the process of mode conversion between acoustic and magnetic waves.

Standard ray theory fails in three circumstances:

(i) in the neighbourhood of caustics (turning points), and in the evanescent regions beyond;
(ii) where the background coefficients vary rapidly; and
(iii) where mode conversion occurs.

Circumstance (i) may in theory be overcome using classical WKB matching procedures (Bender & Orszag 1978), or recently developed complex ray theory (Chapman et al. 1999), but neither is very practical for our purposes. The recent introduction of Fresnel-zone kernels into time–distance helioseismology ameliorates this difficulty somewhat by widening the zone of applicability, though does not remove it (Couvidat et al. 2004).

Circumstance (ii) is of concern near the surface, particularly due to the sharp spike in the acoustic cut-off frequency seen in Fig. 1. However, as noted by Schmitz & Fleck (1998, 2003), the form of the acoustic cut-off frequency is dependent on the choice of dependent and independent variables in the governing differential equations. The sharp spike displayed in the figure is due to the presence of the H' term in equation (3). Schmitz & Fleck (2003) argue strongly that the use of equations which include this term in ω_c is to be avoided for realistic, and in particular empirical solar models such as Model S.

Circumstance (iii) results from the failure of the WKB ansatz to account for the exchange of energy between supposedly distinct modes in the neighbourhood of avoided crossings of the dispersion curves, or more accurately its assumption that the modes are indeed distinct there. This has been addressed at some length recently by Cally (2005, 2006), in the latter case using the general theory set out in Tracy et al. (2003). However, Cally (2006) is based upon wave equations in a form generalized from equation (2), which was suitable for the simple polytropic models discussed there, but suffers from the acoustic cut-off spike problem for the more realistic atmospheres which concern us here. To overcome this, we now present an alternative formulation, more in keeping with the variational foundations of the Tracy et al. (2003) method, and the matrix description of standard MHD ray theory of Weinberg (1962).

We begin with the self-adjoint formulation of linear MHD (Goedbloed & Poedts 2004), which has the advantage that it automatically yields a Hermitian dispersion matrix, and therefore a real dispersion

[5] It should be noted though that our MMMS models feature an infinitely extended temperature minimum region at the top, and that the addition of a more realistic chromosphere will certainly change some results at larger z.

relation. This is appropriate for a dissipationless system, and convenient for use in ray theory. It is to be contrasted with the complex dispersion relation for gravitationally stratified MHD derived previously by McLellan & Winterberg (1968) (see also Thomas 1983).

Using the equilibrium equation $-\nabla p + \rho \boldsymbol{g} + \boldsymbol{j}\times\boldsymbol{B} = \boldsymbol{0}$, where $\boldsymbol{j}$ is the current density, the potential energy may be written as

$$\begin{aligned} W &= -\frac{1}{2}\int \boldsymbol{\xi}^*\cdot\boldsymbol{F}(\boldsymbol{\xi})\,\mathrm{d}V \\ &= \frac{1}{2}\int \rho c^2\,|\nabla\cdot\boldsymbol{\xi}|^2 + |\boldsymbol{b}|^2 + \frac{1}{2}\rho\boldsymbol{g}\cdot\left(\boldsymbol{\xi}\nabla\cdot\boldsymbol{\xi}^* + \boldsymbol{\xi}^*\nabla\cdot\boldsymbol{\xi}\right) \\ &\quad + \frac{1}{2}\boldsymbol{g}\cdot\left(\boldsymbol{\xi}\nabla\cdot\rho\boldsymbol{\xi}^* + \boldsymbol{\xi}^*\nabla\cdot\rho\boldsymbol{\xi}\right) \\ &\quad + \frac{1}{2}\boldsymbol{j}\cdot\left(\boldsymbol{\xi}\times\boldsymbol{b}^* + \boldsymbol{\xi}^*\times\boldsymbol{b}\right) \\ &\quad + \frac{1}{2}\boldsymbol{j}\times\boldsymbol{B}\cdot\left(\boldsymbol{\xi}\nabla\cdot\boldsymbol{\xi}^* + \boldsymbol{\xi}^*\nabla\cdot\boldsymbol{\xi}\right)\,\mathrm{d}V, \end{aligned} \tag{7}$$

where $\boldsymbol{F}$ is the force per unit volume, $\boldsymbol{b} = \nabla\times(\boldsymbol{\xi}\times\boldsymbol{B})$ is the magnetic field perturbation and $\boldsymbol{B}$ is the background field. Specializing now to the uniform field case, where $\boldsymbol{j} = \boldsymbol{0}$, defining $\boldsymbol{X} = \rho^{1/2}\,\boldsymbol{\xi}$ and $Y = \xi\cos\theta - \zeta\sin\theta$, and performing some algebraic manipulations, the associated Lagrangian density is found to be

$$\begin{aligned} \mathcal{L} &= \frac{1}{2}|\dot{\boldsymbol{X}}|^2 - \frac{1}{2}c^2\left|\nabla\cdot\boldsymbol{X} + \frac{X_z}{2H}\right|^2 - \frac{1}{2}\rho a^2|\nabla\times(Y\,\hat{\boldsymbol{e}}_y)|^2 \\ &\quad -\frac{1}{2}\boldsymbol{g}\cdot(\boldsymbol{X}\nabla\cdot\boldsymbol{X}^* + \boldsymbol{X}^*\nabla\cdot\boldsymbol{X}). \end{aligned} \tag{8}$$

The wave equations may be recovered from the variation of the action $\int \mathcal{L}\,\mathrm{d}V\,\mathrm{d}t$ with respect to $\boldsymbol{\xi}$ (Friedland & Kaufman 1987).

Retaining the density derivative in the acoustic term so as to recover the Brunt–Väisälä and acoustic cut-off effects, we now make the formal identification $\nabla \equiv \mathrm{i}\boldsymbol{k}$ and $\partial/\partial t \equiv -\mathrm{i}\,\omega$ (see Tracy & Kaufman 1993, for a rigorous discussion of the application of a 'local Fourier transform' in the context of mode conversion theory). Then, setting $\chi = \nabla\cdot\boldsymbol{X} = \mathrm{i}k_x\rho^{1/2}\xi + \mathrm{i}k_z\rho^{1/2}\zeta$, and solving for ξ and ζ in terms of χ and Y, $\mathcal{L}$ becomes a Hermitian quadratic form in these two variables, $\mathcal{L} = \boldsymbol{Q}^{\mathrm{H}}\tilde{\mathbf{D}}\boldsymbol{Q}$, where $\boldsymbol{Q} = (\chi, Y)^{\mathrm{T}}$, $K = |\boldsymbol{k}|$ the superscript 'H' denotes the Hermitian transpose, and

$$\tilde{\mathbf{D}} = \begin{pmatrix} \tilde{D}_a & \tilde{\eta} \\ \tilde{\eta}^* & \tilde{D}_b \end{pmatrix} \tag{9}$$

is the dispersion matrix, where

$$\tilde{D}_a = \omega^2 - c^2k_\parallel^2 - \omega_{\mathrm{ci}}^2\cos^2\theta,\ \ \tilde{D}_b = \omega^2 - a^2k_\parallel^2 - \omega_{\mathrm{ci}}^2\frac{k_x^2}{K^2} \tag{10}$$

and

$$\tilde{\eta} = \frac{-\mathrm{i}k_\perp\omega^2 + \mathrm{i}k_x\omega_{\mathrm{ci}}^2\cos\theta - gk_xk_\parallel + \frac{1}{2}k_xk_\parallel c^2H^{-1}}{K}. \tag{11}$$

Here, $k_\parallel = k_x\sin\theta + k_z\cos\theta$ and $k_\perp = k_x\cos\theta - k_z\sin\theta$ are the components of the wavevector parallel and perpendicular to the magnetic field.

Standard ray theory is built on the *dispersion function* $\mathcal{D} = \det\mathbf{D}$, or in this case

$$\begin{aligned} \mathcal{D} &= \omega^4 - (a^2+c^2)K^2\omega^2 + a^2c^2K^2k_\parallel^2 \\ &\quad + c^2N^2k_x^2 - (\omega^2 - a^2K^2\cos^2\theta)\omega_{\mathrm{ci}}^2. \end{aligned} \tag{12}$$

The dispersion relation $\mathcal{D} = 0$ limits solutions to hypersurfaces in frequency–wavevector phase space. In the unstratified limit, $\mathcal{D}$ reduces to the usual magnetoacoustic dispersion function $\omega^4 - (a^2 + c^2)K^2\omega^2 + a^2\,c^2\,K^2k_\parallel^2$, and in the non-magnetic case we have the (almost) expected acoustic dispersion relation $\omega^2 - \omega_{\mathrm{ci}}^2 - c^2K^2 + c^2N^2k_x^2/\omega^2 = 0$.

Why 'almost'? Comparing the acoustic dispersion relation with equation (2), we see that ω_{c} has been replaced with ω_{ci}. Which is correct? Clearly equation (2) has exact sinusoidal solutions in an isothermal atmosphere, since c, ω_{c} and N are uniform there. However, also in that case, $\omega_{\mathrm{c}} = \omega_{\mathrm{ci}}$, and so this test cannot distinguish between these two possibilities. Indeed, with Thomas (1983) and Schmitz & Fleck (1998, 2003), we accept that dispersion relations in inhomogeneous media are not unique. Different choices of variables produce dispersion functions which often differ by terms assumed small in the local Fourier transform applied in their derivation. In principle, these differences can be reconciled at higher order in a WKB hierarchy, but that is irrelevant to ray theory, as only the lowest order (geometrical optics), or second lowest order (physical optics) (Weinberg 1962; Bender & Orszag 1978), approximations of WKB are applied there. Terms such as H' and k_zH are therefore of doubtful validity where they are associated with rapidly varying coefficients. Nevertheless, guided by the above-mentioned exact sinusoidal solution in an isothermal non-magnetic atmosphere, by the clear inconsistency of a form of ω_{c} containing a spike such as is displayed in Fig. 1, and by the desire for a model of the greatest simplicity, the dispersion relation (12) will be adopted here as our 'model'.

$\mathcal{D}$ as defined above has other desirable features. These are brought out by extracting the dispersion relations of the magnetic and the acoustic waves in the asymptotic regimes $a \gg c$ (high in the atmosphere) and $c \gg a$ (deep in the interior). A little algebra and the binomial expansion reveal the following.

(i) $a \gg c$ *magnetic.* This is a fast wave in the overlying atmosphere:

$$\omega^2 - a^2K^2 - c^2k_\perp^2 - \omega_{\mathrm{ci}}^2\sin^2\theta + \frac{c^2N^2k_x^2}{\omega^2} = 0. \tag{13}$$

(ii) $a \gg c$ *acoustic.* The atmospheric slow wave:

$$\omega^2 - c^2k_\parallel^2 - \omega_{\mathrm{ci}}^2\cos^2\theta = 0. \tag{14}$$

(iii) $c \gg a$ *magnetic.* The deep interior slow wave:

$$\omega^2 - a^2K^2\,\frac{c^2k_\parallel^2 + \omega_{\mathrm{ci}}^2\cos^2\theta}{c^2K^2 + \omega_{\mathrm{ci}}^2 - c^2N^2k_c^2/\omega^2} = 0. \tag{15}$$

(iv) $c \gg a$ *acoustic.* The deep interior fast wave:

$$\begin{aligned} \omega^2 &- c^2K^2 - \omega_{\mathrm{ci}}^2 + \frac{c^2N^2k_x^2}{\omega^2} \\ &- a^2K^2\,\frac{c^2k_\perp^2 + \omega_{\mathrm{ci}}^2\sin^2\theta - c^2N^2k_c^2/\omega^2}{c^2K^2 + \omega_{\mathrm{ci}}^2 - c^2N^2k_c^2/\omega^2} = 0. \end{aligned} \tag{16}$$

The expected behaviours are evident; in particular the 'ramp' effect clearly displayed in equation (14), which allows acoustic waves to propagate into the solar atmosphere along inclined magnetic field lines, even at frequencies below the acoustic cut-off but for which $\omega > \omega_{\mathrm{ci}}\cos\theta$ (De Pontieu, Erdélyi & James 2004). The deep slow wave (equation 15) is also field aligned as expected if the ω_{ci} and N terms can be neglected. The slight anisotropies of the fast waves (faster propagation across than along field lines) are also well brought out in these formulae.

With the dispersion function $\mathcal{D}$ specified, the ray paths follow from the usual Hamiltonian equations

$$\frac{\mathrm{d}\boldsymbol{x}}{\mathrm{d}\tau} = \frac{\partial\mathcal{D}}{\partial\boldsymbol{k}},\quad \frac{\mathrm{d}\boldsymbol{k}}{\mathrm{d}\tau} = -\frac{\partial\mathcal{D}}{\partial\boldsymbol{x}},\quad \frac{\mathrm{d}t}{\mathrm{d}\tau} = -\frac{\partial\mathcal{D}}{\partial\omega},\quad \frac{\mathrm{d}\omega}{\mathrm{d}\tau} = \frac{\partial\mathcal{D}}{\partial t} \tag{17}$$

(Weinberg 1962; Barnes & Cally 2001), where τ is a time-like variable which parametrizes the progress of a disturbance along the ray

path. If $\mathcal{D}$ is independent of x and t, k_x and ω remain constant along a ray. However, the vertical wavenumber k_z evolves due to the z dependence of the underlying atmosphere. Note that these ray paths depend only on $\mathcal{D}$, but where and how they split (mode convert) depends on the dispersion matrix, and not just its determinant.

Unfortunately, WKB, and by extension ray theory, fails spectacularly in mode conversion regions. This is because it implies a rigid connectivity of the branches of the dispersion curves $\mathcal{D} = 0$. The classical WKB view is that there is a fast mode and a slow mode. The fast wave is dominated by magnetic characteristics where $a \gg c$ and by acoustic behaviour where $c \gg a$, and the opposite for the slow wave. As discussed extensively in Cally (2005, 2006) though, these two curves typically approach closely near the equipartition depth at which $a = c$. In this neighbourhood, the 'other connectivity', i.e. acoustic-fast with acoustic-slow and magnetic-fast with magnetic-slow, is a priori just as plausible. In fact, both occur in general, with some energy taking each route, depending on just how close the dispersion curve avoided crossing is. The general mode conversion theory of Tracy et al. (2003), which we apply to MHD wave theory here, quantifies this dual connectivity.

The basis of the theory is the dispersion matrix

$$\mathbf{D} = \begin{pmatrix} D_a & \eta \\ \eta^* & D_b \end{pmatrix}. \tag{18}$$

Here, it is assumed that the 'coupling term' η is small compared to D_a and D_b in general, but becomes comparable in conversion regions of phase space. Since $\mathcal{D} = \det \mathbf{D} = D_a D_b - |\eta|^2 \approx D_a D_b$, away from conversion regions, the dispersion relation $\mathcal{D} = 0$ approximately decouples to the two 'independent' modes $D_a = 0$ and $D_b = 0$. In the MHD context, we would like D_a to represent the 'acoustic wave' and D_b the 'magnetic wave', with η quantifying the mode transmission (fast-to-slow or vice versa), which occurs in the neighbourhood of the 'star points' $D_a = D_b = 0$. Then, the transmission coefficient T associated with each star point is found to be

$$T = \exp(-2\pi|\eta|^2/|\mathcal{B}|)_\star, \tag{19}$$

where

$$\mathcal{B} = \{D_a, D_b\} = \frac{\partial D_a}{\partial k_z}\frac{\partial D_b}{\partial z} - \frac{\partial D_b}{\partial k_z}\frac{\partial D_a}{\partial z} \tag{20}$$

is the Poisson bracket of the uncoupled dispersion functions, and the subscripted star indicates that T must be evaluated where $D_a = D_b = 0$. These formulae are presented in Tracy et al. (2003; equations 22 and 23), and derive from a complex mathematical process involving linear canonical transformations in phase space (Tracy & Kaufman 1993) and subsequent matching of asymptotic WKB solutions across the mode conversion region. We emphasize that $T = 0$ (i.e. $\eta \to \infty$) corresponds to no transmission (tunnelling) through the star point from fast to slow, or vice versa, and $T = 1$ ($\eta = 0$) to *total transmission*. $T = 0$ is (fallaciously) implicit in the standard WKB theory, where fast and slow modes maintain their identities throughout.

Unfortunately, $\tilde{\mathbf{D}}$ as defined in equations (9)–(11) is not suitable for our purposes, as $\tilde{D}_a$ and $\tilde{D}_b$ do not represent the two independent modes asymptotically. This is easily rectified though with a change of variable $\boldsymbol{Q} = \mathbf{A}\boldsymbol{R}$, with $\boldsymbol{R}$ being the new 2-vector dependent variable and $\mathbf{A}$ is a 2×2 non-singular matrix. Then $\mathcal{L} = \boldsymbol{R}^{\mathrm{H}}\mathbf{D}\boldsymbol{R}$, where $\mathbf{D} = \mathbf{A}^{\mathrm{H}}\tilde{\mathbf{D}}\mathbf{A}$. Rather than specify $\mathbf{A}$ directly, we define it by specifying D_a and D_b, together with the requirement that $\det \mathbf{D} = \det \tilde{\mathbf{D}} = \mathcal{D}$, i.e. the dispersion function is unchanged. We choose D_a and D_b based on a smooth matching of the $a \ll c$ and $a \gg c$ acoustic and magnetic branches as set out in equations (13)–(16), respectively:

$$\begin{aligned} D_a = {} & \omega^2 - c^2K^2 + \frac{1+U}{2}\left(c^2k_\perp^2 - \omega_{\mathrm{ci}}^2\cos^2\theta\right) \\ & -\frac{1-U}{2}\left(\omega_{\mathrm{ci}}^2 - \frac{c^2N^2k_x^2}{\omega^2}\right. \\ & \left. + a^2K^2\,\frac{c^2k_\perp^2 + \omega_{\mathrm{ci}}^2\sin^2\theta - c^2N^2k_c^2/\omega^2}{c^2K^2 + \omega_{\mathrm{ci}}^2 - c^2N^2k_c^2/\omega^2}\right) \end{aligned} \tag{21}$$

and

$$\begin{aligned} D_b = {} & \omega^2 - a^2K^2 - \frac{1+U}{2}\left(\omega_{\mathrm{ci}}^2\sin^2\theta + c^2k_\perp^2 - \frac{c^2N^2k_x^2}{\omega^2}\right) \\ & +\frac{1-U}{2}\,a^2K^2\,\frac{c^2k_\perp^2 + \omega_{\mathrm{ci}}^2\sin^2\theta - c^2N^2k_c^2/\omega^2}{c^2K^2 + \omega_{\mathrm{ci}}^2 - c^2N^2k_c^2/\omega^2}, \end{aligned} \tag{22}$$

where U rises smoothly and monotonically from -1 at $a = 0$ to 1 at $c = 0$. We find that a good choice is $U = (a^4 - c^4)/(a^4 + c^4)$.

The procedure set out above for choosing the forms of D_a and D_b is not entirely unique, but none the less is severely constrained by the requirement that these two 'reduced' dispersion functions closely model the magnetic and acoustic branches away from the conversion region. The numerical results of Section 5 illustrate just how well this choice of D_a and D_b performs in this regard. Different choices of the ramp function U alter the results only slightly, and make no practical difference.

That such a transformation is possible is guaranteed by Sylvester's law of inertia (Horn & Johnson 1985), at least in the region between the two dispersion curves, which is the only place we need it (see Fig. 11). Sylvester's law states that any two Hermitian matrices are *congruent (i.e. may be connected by a transformation of the form $\mathbf{D} = \mathbf{A}^{\mathrm{H}}\tilde{\mathbf{D}}\mathbf{A}$) provided they have the same inertia. The *inertia* of a Hermitian matrix is the ordered triple consisting, respectively, of the number of positive, negative, and zero eigenvalues (recall that all eigenvalues of a Hermitian matrix are real). Now since the determinant $\mathcal{D}$ of $\mathbf{D}$ and $\tilde{\mathbf{D}}$ is equal to the product of their eigenvalues, $\lambda_1\lambda_2 = \mathcal{D} = \tilde{\lambda}_1\tilde{\lambda}_2$, and since $\mathcal{D} < 0$ between the dispersion curves (and hence in the neighbourhood of the star points), it follows that the inertia is (1, 1, 0) in both cases. $\mathbf{D}$ and $\tilde{\mathbf{D}}$ are therefore *congruent.

It then remains to determine η, or rather $|\eta|^2$, which is all that matters in calculating transmission coefficients (equation 19). The phase of the 'converted' (i.e. acoustic-to-magnetic or

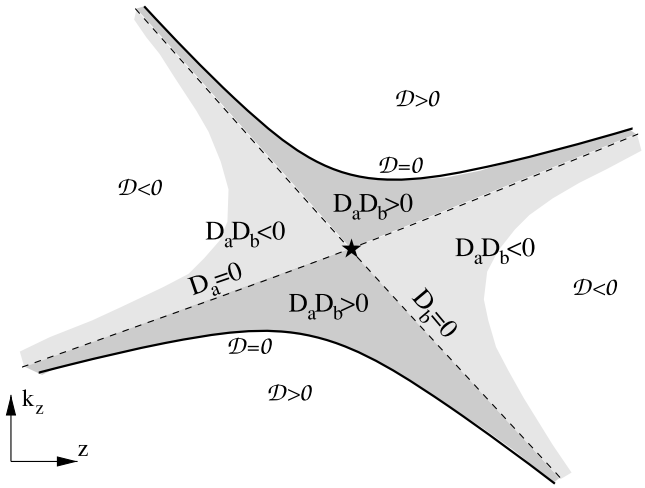

Figure 11. Schematic diagram of the typical interaction region in z–k_z phase space surrounding a star point.

magnetic-to-acoustic) ray does depend on arg η (Tracy et al. 2003; equation 22), but is not of concern here. Clearly, $|\eta|^2$ follows using the equality of determinants

$$|\eta|^2 = D_a D_b - \mathcal{D}. \tag{23}$$

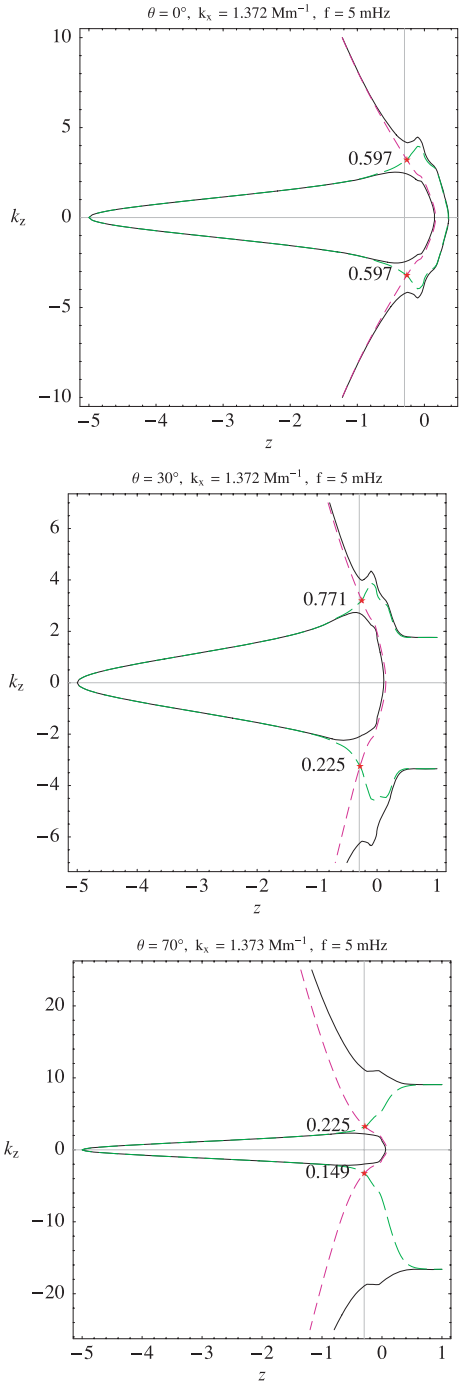

Figure 12. The z–k_z dispersion diagrams $\mathcal{D} = 0$ (full curves) for the three cases of Fig. 3, i.e. $\theta = 0°$, 30° and 70°. In each case, the full fast mode lobe is shown, extending down to the natural cavity depth at $z = -5$ Mm. The slow mode branch is represented by the other full curve. The dashed curves correspond to $D_a = 0$ and $D_b = 0$, and the 'star points' at which they cross may be thought of as the 'transmission points' through which fast–slow and slow–fast tunnelling occurs. The transmission coefficients for each star point are superimposed on the figures. The vertical grey line indicates the position of the $a = c$ equipartition level.

At star points $D_a = D_b = 0$, which are the only positions in phase space where we need η, it follows of course that

$$|\eta|^2_\star = -\mathcal{D}. \tag{24}$$

It is instructive to explore the case where the cut-off and buoyancy effects may be neglected, $\omega_{ci} = N = 0$. Then the star points occur exactly at $a = c$, $K^2 = \omega^2/c^2$ in phase space, and so

$$|\eta|^2_\star = c^4 K^2 k_\perp^2. \tag{25}$$

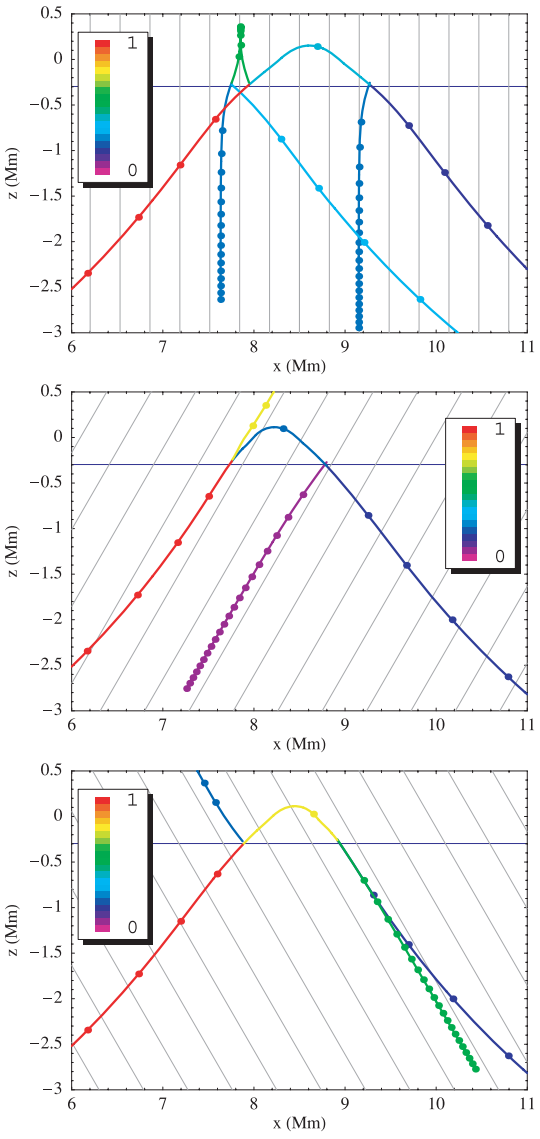

Figure 13. Ray path diagrams in physical x–z space for 5-mHz acoustic rays launched horizontally from $x = 0$, $z = -5$ Mm in the presence of a 2-kG magnetic field which is vertical (top panel), inclined at 30° (middle panel) and at −30° (bottom panel). The grey-scale legend associates black to full energy, and light grey to no energy. Of these three cases, most conversion to a slow acoustic mode travelling into the atmosphere occurs when $\theta = 30°$. The horizontal line at $z \approx -0.3$ Mm indicates the equipartition level at which the Alfvén and sound speed coincide, which is close to the level of mode transmission between fast and slow waves. The dots on the ray paths represent 1-min time intervals, making it easy to distinguish fast from slow branches. The background straight grey lines represent the magnetic field.

The associated transmission coefficient may then be shown to be

$$\begin{aligned} T &= \exp\left[-\frac{\pi h K^2 k_\perp^2}{|k_z|\,(K^2+k_\perp^2)}\right]_{a=c} \\ &\approx \exp\left(-\frac{\pi h k_\perp^2}{|k_z|}\right)_{a=c} \quad \text{for} |k_\perp| \ll K \\ &= \exp\left[-\pi K h_s \sin^2\alpha\right]_{a=c}, \end{aligned} \tag{26}$$

where $\alpha = \arcsin(k_\perp/K)$ is the *attack angle*. Here, $h = [\mathrm{d}\,(a^2/c^2)/\mathrm{d}\,z]^{-1}_{a=c}$ is the equipartition layer scaleheight, i.e. a measure of the thickness of the layer over which $a \approx c$, and $h_s = [\mathrm{d}\,(a^2/c^2)/\mathrm{d}\,s]^{-1}_{a=c}$ is the layer thickness as measured along the oblique path with direction $\hat{\boldsymbol{k}}$, i.e. the direction of the phase velocity. Thus, fast-to-slow or slow-to-fast transmission is enhanced by any or all of: (i) fine attack angle; (ii) small wavenumber (low frequency); and (iii) thin equipartition layer. In the WKB limit $Kh_s \gg 1$, we recover $T \to 0$ except effectively at exactly $\alpha = 0$. This is in accord with the usual WKB understanding that the fast and slow modes are decoupled save for parallel propagation at $a = c$. For finite Kh_s though, significant energy transmission occurs for attack angles $|\sin\alpha| \lesssim 1/\sqrt{\pi K h_s}$. The significance of attack angle has been noticed in numerical simulations previously (Bogdan et al 2003).

Reintroduction of ω_{ci} and N complicates and modifies these conclusions, in particular moving the star point slightly away from $a = c$, and preventing T from reaching 1 even at $\alpha = 0$, but does not fundamentally change them.

The role of the attack angle is crucial in understanding Figs 3–5.

5 PHYSICAL INSIGHTS FROM RAY CONVERSION THEORY

The most striking result from the wave mechanical experiment of Section 3 is that the acoustic energy and acoustic flux in the low solar atmosphere of active regions should be very dependent on magnetic field inclination. On the other hand, to be more precise, the surface magnetic field acts as a filter on the ensemble of helioseismic waves below the surface, preferentially allowing through certain waves. How are we to understand this? Clearly, the concept of *attack angle* is relevant, and in this section we try to qualitatively explain the wave mechanical results using insights from ray theory.

Dispersion diagrams for the three scenarios represented in Fig. 3 are shown in Fig. 12, and the corresponding physical space ray paths for the $\theta = 0^\circ$ and $\pm 30^\circ$ cases in Fig. 13. Again, the frequency is 5 mHz and the horizontal wavenumber k_x is chosen so that the ray has lower turning point at $z = -5$ Mm. The dispersion diagrams display the loci of the dispersion relation $\mathcal{D} = 0$ (see equation 12 in z–k_z space. The closed lobe represents the fast wave, with upper and lower turning points at $z \approx 0$ and $z = -5$ Mm, respectively (see Fig. 14). The other branch is the slow mode. The top panel shows dispersion curves for a vertical magnetic field, the middle panel is for a magnetic field inclined at $\theta = 30^\circ$ and the bottom panel is for a magnetic field inclined at $\theta = 70^\circ$, all with $B = 2$ kG. The star points at which mode transmission between the two branches occur are indicated by a small star, and their associated transmission coefficients $0 \leqslant T \leqslant 1$ displayed beside them. We initially launch a fast ray horizontally from the lower turning point, and trace the path in a clockwise direction. If, instead of following a ray moving clockwise about the fast lobe, we proceed anticlockwise, this is equivalent to a ray moving in the opposite horizontal direction, and hence to the case with the sign of θ reversed.

When the field is vertical, the diagram, and hence T, is symmetric on the upward and downward legs. At this frequency (5 mHz), the slow mode locus is closed at the top, since it is less than the atmospheric acoustic cut-off frequency of about 5.09 mHz in the 2-kG MMMS model. Hence, the slow acoustic wave produced by mode transmission at the first star point is reflected back down undergoing further partial transmission on the next close encounter with a star point (Fig. 13, top panel).

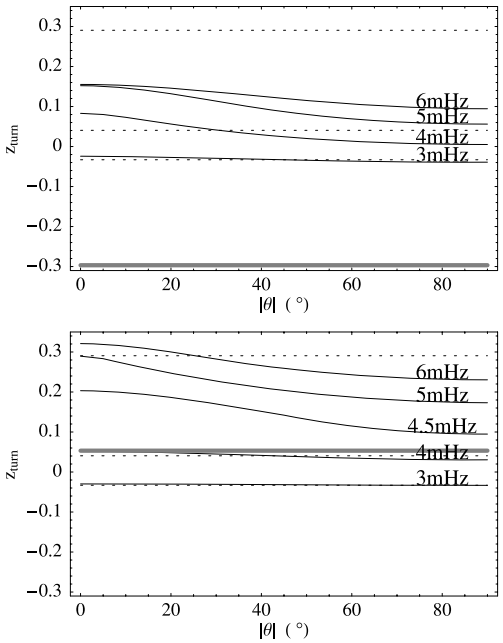

Figure 14. The upper turning depth of fast rays with various frequencies (as labelled), as functions of magnetic field inclination θ. Top panel: $B =$ 2-kG magnetic field; bottom panel: $B = 1$ kG. The dotted horizontal lines represent the non-magnetic case for 3, 4 and 5 mHz (there is no upper turning point at 6 mHz). The thick horizontal grey line indicates the equipartition depth at which $a = c$.

However, for a moderately inclined field ($\theta = 30^\circ$), T is significantly enhanced at the first star point due to the fine attack angle, allowing the majority (77 per cent) of energy to transmit, or mode convert, from a fast acoustic to a slow acoustic wave. In addition, at this inclination, the ramp effect has come into play and the slow acoustic locus is now open at the top, meaning that slow rays are free to propagate up into the atmosphere. Of the energy remaining in the fast mode beyond the first star point (23 per cent), a further 23 per cent (total 5 per cent) then transmits to the slow branch on the downward leg. When very high inclinations are reached ($\theta = 70^\circ$), there is very little conversion at either star point because of the large attack angle. The amount of fast-to-slow transmission is dependent on the magnetic field angle (see Fig. 15), and particularly on the sign of θ.

From this discussion, we have learned that the crucial issue determining how much acoustic (slow) energy progresses into the overlying atmosphere is the strength of the first star point. For this reason, we call this star point the *gatekeeper*. Energy staying on the fast branch refracts back downward and can only influence the atmosphere above through its evanescent tail (not accounted for by ray theory). On the other hand, the slow ray, provided the slow branch is open due to $\omega > \omega_{ci}\cos\theta$, propagates upward into the atmosphere along field lines, and does not refract.

The top panel of Fig. 13 corresponds to the top panel of Fig. 12. The vertical field shows conversion occurring at three locations: (i) the first encounter (gatekeeper) with the equipartition depth where most energy transmits into the slow ray, (ii) the reflected slow

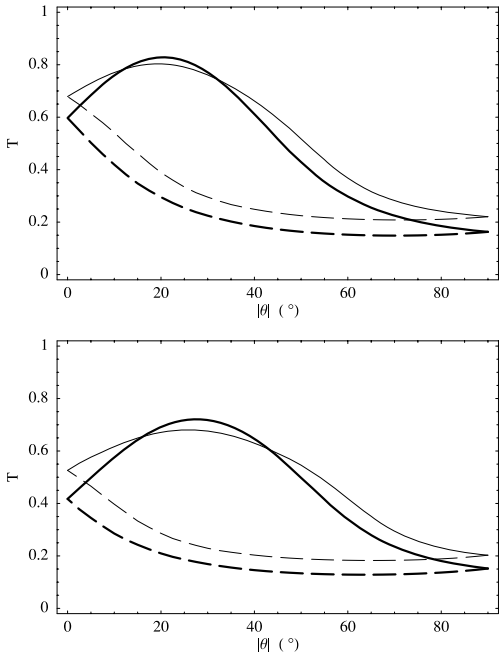

Figure 15. Top panel: transmission coefficient of the gatekeeper star point at various inclinations of 2-kG magnetic field for fast rays with lower turning point at $z_1 = -5$ Mm. Lower panel: same, but for shallower rays with $z_1 = -3$ Mm. The thick curves represent 5-mHz wave frequency, and the thin lines 4 mHz. Solid curves: $\theta > 0$; dashed curves: $\theta < 0$.

acoustic ray converting most of its energy into a fast acoustic ray and (iii) the continued fast ray converting strongly to slow on the downward leg. At $\theta = 30^\circ$ (the middle panel), we see most energy is converted to a slow acoustic mode travelling up into the atmosphere, due to the ramp effect, guided by the magnetic field lines. The second star point corresponds to where the ray splits for the second time, and the fast magnetic mode only weakly undergoes transmission to a slow magnetic mode, which is again guided by the field but this time into the deep interior. The contrasting case is depicted in the bottom panel of Fig. 13 where $\theta = -30^\circ$ corresponds to the middle panel of Fig. 12 but with the fast lobe traversed in an anticlockwise sense. Now, we see very little transmission at the gatekeeper (lower star point in this case). Most of the ray energy continues as a fast magnetic wave until it undergoes strong transmission again on the downward leg where the slow magnetic wave (of significant energy) is field guided down into the interior. With a fine attack angle, there is a significant amount of transmission, and with a large attack angle there is little transmission. When the attack angle is large, the second encounter with the equipartition depth induces greater transmission to a slow acoustic ray, but this time it is channelled out of the acoustic wave field and down into the interior along the magnetic field lines. Overall, it is very clear again that the upgoing atmospheric slow wave is most pronounced for $\theta = 30^\circ$ of the cases displayed, emphasizing the importance of a strong gatekeeper, i.e. fine attack angle, if substantial acoustic energy is to propagate into the atmosphere. (In the middle panel, it is seen that the ray at the first conversion point is indeed nearly parallel to the magnetic field. Although attack angle is defined in terms of the direction of the *phase* velocity rather than the group velocity, or ray direction, this is still indicative of a small α and hence large T.)

Transmission may not always occur. When the magnetic field is weak, the geometrical height of the equipartition depth is raised and the ray may not encounter the equipartition layer before reflecting off the acoustic cut-off (see Fig. A2 in Appendix A). Fig. 14 displays the fast wave upper turning depth in 1- and 2-kG magnetic fields for different frequencies, and compares it to the non-magnetic case. It also shows the depth of the equipartition layer (thick line). Clearly, at 2 kG, the fast ray at all relevant frequencies passes through $a = c$ and is subject to fast-to-slow mode conversion. However, at 1 kG, this is so only above about 4 mHz. In all cases, the effect of θ on turning depth is minor, especially at the lower frequencies. (The frequency dependence of turning depth results primarily from the $\omega_{\rm ci}^2 \sin^2\theta$ term in equation 13.)

When mode conversion does occur though, we find a strong dependency on the inclination of the magnetic field because of attack angle. Fig. 15 plots T against $|\theta|$ for 4- and 5-mHz rays in a 2-kG magnetic field. The transmission for positive θ peaks at around 20°–22° in these cases for rays with lower turning point at $z_1 = -5$ Mm. Although we are not exactly comparing like with like,[6] reference to the acoustic flux curves in Fig. 4 shows that this is very much in accord with the wave mechanical calculations. For shallower waves ($z_1 = -3$ Mm), the peaks occur at slightly higher θ, consistent with the lower panel of Fig. 4, and with the idea that attack angle is crucial: shallower skimming rays naturally meet the equipartition level at greater angle to the vertical, and are therefore more susceptible to mode transmission in more highly inclined field.

Ray considerations also broadly explain the results of Figs 5 and 6, which show peak acoustic energy density in the atmosphere for moderate positive magnetic field inclinations when $\omega > \omega_{\rm ci} \cos\theta$, i.e. when the slow mode is propagating rather than evanescent there.

6 DISCUSSION

Mode conversion is the most likely candidate for describing acoustic energy 'absorption' in sunspots (Cally et al. 2003; Crouch et al. 2005). Most previous modelling of this effect has focused on conversion to downgoing slow modes, whereby energy is lost from the acoustic field to essentially Alfvénic oscillations in the interior (though see Cally et al. 1994, for a discussion of upward losses in vertical magnetic field). However, at least above the (ramp reduced) acoustic cut-off frequency, energy may also propagate upwards into the overlying atmosphere (e.g. Brynildsen et al. 2002; De Moortel et al. 2002), with observationally testable consequences.

We are now entering a phase where we can begin to compare theory with observations of the low atmosphere made with instruments such as SOHO/MDI, and in the near future the Solar Dynamics Observatory/Helioseismic and Magnetic Imager (SDO/HMI). The latter will prove particularly valuable because of its ability to generate vector magnetograms as well as Doppler data. Specifically, an explanation of the observational results of Schunker et al. (2005) in sunspot penumbrae, where magnetic field *direction* is found to have a significant influence on the correlation between acoustic ingression (the incoming driver) and MDI-observed atmospheric vector velocities, is seemingly within reach.

Based on the wave mechanical results of Section 3, and the insights from ray conversion theory in Sections 4 and 5, we

[6] The vertical component of acoustic flux in the atmosphere obviously depends crucially on the strength of fast-to-slow mode conversion, but also on the geometric $\cos\theta$ effect resulting from the flux being field aligned. This is partly responsible for the drop-off in vertical flux as θ increases beyond the peak in Fig. 4, though the major effect is the variation of T with θ. Furthermore, at small inclinations where the ramp effect has not yet opened up the slow branch, there is zero flux reaching high into the atmosphere, despite T being non-zero.

would expect to see evidence of mode conversion in MDI surface velocity alignment with magnetic field direction. It is clear that MDI is observing at a height well above the equipartition level, and that upcoming helioseismic waves penetrate to the conversion level near $a = c$ for larger field strengths (≈ 2 kG) at all relevant frequencies, and for moderate field strengths (≈ 1 kG) at higher frequencies ($\gtrsim 4$ mHz). Furthermore, waves converted from fast to slow by this process should then propagate upward to and beyond the height of MDI observation provided the frequency exceeds the ramp-reduced acoustic cut-off. 5-mHz observations are particularly relevant here. Below the acoustic cut-off, at low frequency or small θ, the slow wave is evanescent (the fast wave always is) and so decays with height. Nevertheless, even when the slow mode is evanescent [see $-20^\circ \lesssim \theta \lesssim 35^\circ$ in the lower panel in Fig. 9 and note that $\arccos(\omega/\omega_{\rm ci}) = 38^\circ$ in this 4-mHz case] quite close field alignment is expected at low heights. Preliminary observational determination of velocity ellipse characteristics has only been carried out at 5 mHz so far (Schunker et al. 2006), with the results indicating generally high eccentricity, but substantial deviation from field alignment. This is compatible with theory provided a^2/c^2 is not too large at the observation height. (The putative height of formation of the MDI Ni I is around 200 km in quiet Sun, but may be of the order of 100 km lower in sunspot penumbrae due to the Wilson depression, though we are unaware of any detailed modelling to confirm this.)

In reality, we are observing a three-dimensional magnetic field with a combination of travelling and evanescent waves from all directions impinging upon the magnetic field. Figs 12 and 13 show that the energy which reaches heights similar to MDI observation (although a direct geometric connection between model and sunspot is highly dubious) is dominated by field-guided velocity. Observations will thus depend upon transmission occurring and the ray propagating to observational heights. In situations where the attack angle is fine and there is significant transmission to a slow acoustic ray travelling into the atmosphere, we would expect to observe field-guided velocities, for instance Fig. 13 (middle panel). At this stage, our theoretical results are limited to the 2D plane in which the magnetic field lies. Nevertheless, interpretation in terms of attack angle allows us to surmise that rays approaching from out of this plane will be less strongly transmitted as slow waves into the atmosphere. Overall, we expect that strong surface field acts as a filter on this subsurface wave ensemble, preferentially selecting for transmission rays with phase velocity in a cone closely aligned to the magnetic field direction.

The maximal transmission occurring at $\theta \approx 22^\circ$ is in accordance with the wave mechanical description of Crouch & Cally (2003) who find the minimal extinction length (maximal absorption) exists close to the $\theta = 25^\circ$ mark. A fine attack angle (positive θ) is responsible for large transmission coefficients, allowing a significant proportion of the ray energy to convert to a slow acoustic wave. Then, if the ramp effect is operative, this energy is field guided up into the atmosphere. The situations primarily responsible for extracting energy from the near surface by field guiding the slow ray down into the deep interior are when there exists a large attack angle (negative θ) and when the slow ray has been reflected off the acoustic cut-off as in Fig. 13 bottom and top panels, respectively.

A concern with using ray theory near the solar surface, be it in quiet Sun or active region, is the non-uniqueness of the acoustic cut-off frequency. This suggests that direct comparison between ray and wave mechanical calculations is unlikely to yield much better than qualitative correspondence there. The fact that time–distance helioseismology typically uses Model S or similar together with the Deubner & Gough form of the acoustic cut-off frequency, equation (3), is concerning, because there is considerable uncertainty about the exact reflection height (so far as that concept is meaningful in a non-WKB medium), and consequently uncertainty in ray traveltimes.

Furthermore, judging by a comparison of Figs 4 and 15, ray conversion theory overestimates the degree of fast-to-slow transmission at high θ. This is not surprising. The derivation of equation (19) is based on a local analysis of the neighbourhood of a star point in z–k_z space. As the gap between the fast and slow branches widens, this becomes progressively less appropriate. Small values of T therefore should be regarded as indicative only.

Schunker et al. (2005) observe that the effect of the magnetic field on acoustic rays (deviation of the phase of the correlation between ingression and observed penumbral velocity, $\delta\phi$) is largest at frequencies of 5 mHz rather than 3 mHz, and for stronger magnetic field strength in accord with the outcomes of the mode conversion theory presented here. These results also suggest that the observed velocity must have some kind of dependence upon the magnetic field direction, since the result changes with the angle between the line of sight and the magnetic field. This is also consistent with our theoretical findings (Fig. 9). Observationally, within a sunspot, magnetic field strength and inclination are inseparable. The most pronounced effect is for a strong magnetic field with inclination less than 42°, which is consistent with expectations, but it is not clear whether this is due to the stronger magnetic or the moderate inclination. Conversely, little deviation $\delta\phi$ is seen in observations where the field is weak and highly inclined ($\theta > 66^\circ$), but again, we cannot resolve which of the two characteristics is responsible since both have this effect in theory.

Although ray theory is a useful interpretative tool in the current context, for these and other reasons (e.g. fast mode caustics and evanescence), it is *not* a viable technique for quantitative reconstruction of the entire wave field in the surface layers. Even in the much simpler interior of an adiabatic polytrope, the correspondence between the wave field and ray bundles is complicated and imperfect (Bogdan 1997). Furthermore, complete treatment of mode conversion, including the incorporation of interference effects, would require a much more complicated analysis,[7] which is contrary to the original point of using a ray description rather than direct solution of the wave equations. For all these reasons, it is not appropriate to attempt a quantitative comparison of ray and wave mechanical solutions for the problems addressed here. Nevertheless, qualitative correspondences are stark, compelling and enlightening.

It would be useful to devise some way to do similar calculations to Schunker et al. (2005) isolating waves impinging on a sunspot from one direction. This has not yet been done. It would also be appropriate to increase the reality of the model. Now that ray theory has provided us with insights into the significance of the attack angle, it may be more useful to extend the wave mechanical formalism to three dimensions in a realistic atmosphere and glean results for comparison with observation.

ACKNOWLEDGMENTS

The authors gratefully acknowledge the advice of colleagues Alina Donea, Charlie Lindsey, Jørgen Christensen-Dalsgaard, Bernhard Fleck, Doug Braun and Eric Chu.

[7] Tracy et al. (2003) claim at the end of Section III that the wave field can be reconstructed in the conversion region, and promise details in a future paper. However, this paper has not yet eventuated.

REFERENCES

Balmforth N. J., Gough D. O., 1990, ApJ, 362, 256
Barnes G., Cally P. S., 2001, Publ. Astron. Soc. Aust., 18, 243
Bender C. M., Orszag S. A., 1978, Advanced Mathematical Methods for Scientists and Engineers. McGraw-Hill, New York
Bogdan T. J., 1997, ApJ, 477, 475
Bogdan T. J., Cally P. S., 1997, Proc. R. Soc. A, 453, 943
Bogdan T. J., Brown T. M., Lites B. W., Thomas J. H., 1993, ApJ, 406, 723
Bogdan T. J. et al., 2003, ApJ, 599, 626
Braun D. C., 1995, ApJ, 451, 859
Braun D. C., Lindsey C., 2000, Sol. Phys., 192, 307
Braun D. C., Duvall T. L. Jr, La Bonte B. J., 1987, ApJ, 319, L27
Brynildsen N., Maltby P., Fredvik T., Kjeldseth-Moe O., 2002, Sol. Phys., 207, 259
Cairns R. A., Fuchs V., 1989, Phys. Fluids B, 1, 350
Cairns R. A., Lashmore-Davies C. N., 1983, Phys. Fluids, 26, 1268
Cairns R. A., Lashmore-Davies C. N., 1986, Phys. Fluids, 29, 3639
Cally P. S., 2001, ApJ, 548, 473
Cally P. S., 2005, MNRAS, 358, 353
Cally P. S., 2006, Phil. Trans. R. Soc. A, 364, 333
Cally P. S., Bogdan T. J., 1993, ApJ, 402, 732
Cally P. S., Bogdan T. J., Zweibel E. G., 1994, ApJ, 437, 505
Cally P. S., Crouch A. D., Braun D. C., 2003, MNRAS, 346, 381
Chapman S. J., Lawry J. M. H., Ockendon J. R., Tew R. H., 1999, SIAM Rev., 41, 417
Christensen-Dalsgaard J. et al., 1996, Sci, 272, 1286
Couvidat S., Birch A. C., Kosovichev A. G., Zhao J., 2004, ApJ, 607, 554
Crouch A. D., 2003, PhD thesis, Monash Univ.
Crouch A. D., Cally P. S., 2003, Sol. Phys., 214, 201
Crouch A. D., Cally P. S., 2005, Sol. Phys., 227, 1
Crouch A. D., Cally P. S., Charbonneau P., Braun D. C., Desjardins M., 2005, MNRAS, 363, 1188
De Moortel I., Ireland J., Walsh R. W., 2002, A&A, 387, L13
De Pontieu B., Erdélyi R., James S. P., 2004, Nat, 430, 536
Deubner F.-L., Gough D. O., 1984, ARA&A, 22, 593
D'Silva S., 1996, ApJ, 469, 964
Friedland L., Kaufman A. N., 1987, Phys. Fluids, 30, 3060
Goedbloed H., Poedts S., 2004, Principles of Magnetohydrodynamics. Cambridge Univ. Press, Cambridge
Horn R. A., Johnson C. R., 1985, Matrix Analysis. Cambridge Univ. Press, Cambridge
Khomenko E., Collados M. 2006, ApJ, in press
Kosovichev A. G., Duvall T. L. Jr, Scherrer P. H., 2000, Sol. Phys., 192, 159
Maltby P., Avrett E. H., Carlsson M., Kjeldseth-Moe O., Kurucz R. L., Loeser R., 1986, ApJ, 306, 284
Mathew S. K., Solanki S. K., Lagg A., Collados M., Borrero J. M., Berdyuginau S., 2004, A&A, 422, 693
McLellan A., Winterberg F., 1968, Sol. Phys., 4, 401
Mickey D. L., Canfield R. C., Labonte B. J., Leka K. D., Waterson M. F., Weber H. M., 1996, Sol. Phys., 168, 229
Rosenthal C. S., Julian K. A., 2000, ApJ, 532, 1230
Schmitz F., Fleck B., 1998, A&A, 337, 487
Schmitz F., Fleck B., 2003, A&A, 399, 723
Schunker H., Braun D. C., Cally P. S., Lindsey C., 2005, ApJ, 621, L149
Schunker H., Braun D. C., Cally P. S., Lindsey C., 2006, in Leibacher J., Uitenbroek H., Stein R., eds, ASP Conf. Ser., Vol. 23, Solar MHD: Theory and Observations – a High Spatial Resolution Perspective. Astron. Soc. Pac., San Francisco (in press)
Spruit H. C., 1991, in Toomre J., Gough D. O., eds, Lecture Notes in Physics, Vol. 388, Challenges to Theories of the Structure of Moderate Mass Stars. Springer-Verlag, Berlin, p. 121
Spruit H. C., Bogdan T. J., 1992, ApJ, 391, L109
Swanson D. G., 1998, Theory of Mode Conversion and Tunneling in Inhomogeneous Plasmas. Wiley, New York
Thomas J. H., 1983, Ann. Rev. Fluid Mech., 15, 321
Tracy E. R., Kaufman A. N., 1993, Phys. Rev. E, 48, 2196
Tracy E. R., Kaufman A. N., Brizard A. J., 2003, Phys. Plasmas, 10, 2147
Unno W., Osaki Y., Ando H., Saio H., Shibahashi H., 1989, Nonradial Oscillations of Stars, 2nd edn. Univ. Tokyo Press, Tokyo
Weinberg S., 1962, Phys. Rev., 126, 1899
Zhugzhda Y. D., Dzhalilov N. S., 1982, A&A, 112, 16
Zhugzhda Y. D., Dzhalilov N. S., 1984, A&A, 132, 45

APPENDIX A: MAGNETICALLY MODIFIED MODEL S

Model S of Christensen-Dalsgaard et al. (1996) provides a convenient description of the surface layers of the quiet Sun. Unfortunately, no similar model is available for sunspot penumbrae. However, we may crudely construct one from Model S by taking into account the effects of magnetic field. Following the lead of Mathew et al. (2004) in ignoring tension effects and setting $p_g = p_0 - p_m$, where $p_0(z)$ is the pressure in Model S and p_g and p_m are the gas and magnetic pressures in the new model, and ignoring variations in p_m with height in comparison with those in p_g, a new sound speed profile is given by

$$c^2 = c_0^2 - \frac{\Gamma_1}{2}a^2, \tag{A1}$$

where $a^2 = B^2/\mu\rho$. Here, hydrostatic equilibrium has been applied to show that the density profile $\rho(z)$ is not altered by the introduction of a uniform (or indeed any force free) magnetic field. Furthermore, variations in the adiabatic index Γ_1 due to ionization differences between the models have been ignored (see Crouch et al. 2005, where this is taken into account).

Clearly though, equation (A1) is only plausible where there is a lateral force balance between 'inside' and 'outside'. It is not

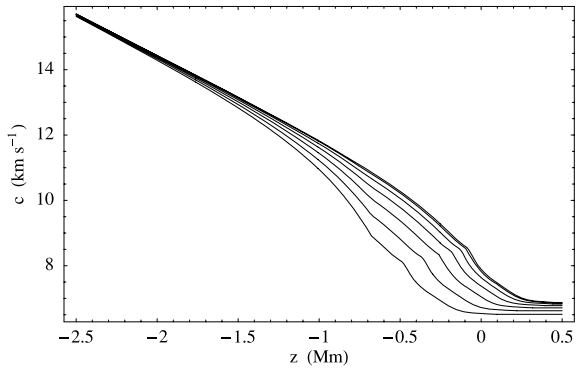

Figure A1. The sound speed c against z for the MMMS with field strengths 0, 0.5, 1, 1.5, 2, 2.5 and 3 kG (right to left).

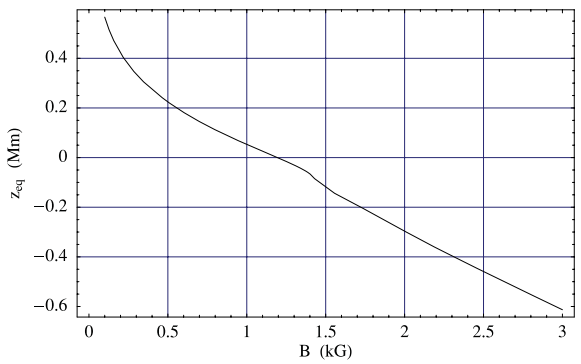

Figure A2. The equipartition level z_{eq} (Mm) as a function of magnetic field strength B (kG) in the MMMS.

appropriate above the surface where magnetic canopy expands to fill the available space. We therefore modify equation (A1) by taking into account both the reduced temperature in a spot, and the Wilson depression of around 400 km in umbrae and 100–120 km in penumbrae (Mathew et al. 2004). Judging by the umbral models of Maltby et al. (1986), the minimum umbral temperature is cooler than in the quiet Sun reference model by typically around 10 per cent. Assuming that this effect and the depth of the Wilson depression scale linearly with magnetic energy density, the following ad hoc model represents a reasonable representation of the expected structure:

$$c^2 = \max\left[c_0^2 - \frac{\Gamma_1}{2}a^2,\ \left(1 - \frac{B^2}{10B_0^2}\right)c_0^2\left(z + 0.4B^2/B_0^2\right)\right], \quad \text{(A2)}$$

where $B_0 = 3$ kG is a reference field strength characteristic of umbrae. We do not model the chromospheric increase in temperature at higher levels. This sound speed is plotted in Fig. A1 for various magnetic field strengths.

With the MMMS in place then, it is possible to determine the equipartition height $z_{\rm eq}$ as a function of field strength. Fig. A2 shows that at penumbral strengths, 1–2 kG, we might expect $-0.3 \lesssim z_{\rm eq} \lesssim 0.05$ Mm. This strongly favours substantial near-surface magnetic effects on helioseismic waves in penumbrae. In umbrae, $z_{\rm eq}$ could be as deep as -0.6 Mm according to this model.

This paper has been typeset from a TEX/LATEX file prepared by the author.